Towards Large Eddy Simulation of Non-Homogeneous Particle Laden Turbulent Gas Flows Using Euler-Euler Approach

Eleonore Riber	Mathieu Moreau	Olivier Simonin	Bénédicte Cuenot
CERFACS	IMFT	IMFT	CERFACS
42 Av. G. Coriolis	Av. C. Soula	Av. C. Soula	42 Av. G. Coriolis
31057 Toulouse	31400 Toulouse	31400 Toulouse	31057 Toulouse
riber@cerfacs.fr	mmoreau@imft.fr	simonin@imft.fr	cuenot@cerfacs.fr

Abstract

A Large Eddy Simulation approach for Eulerian-Eulerian dispersed two-phase flow is presented. It is shown that not only a Sub-Grid Scales term modeling the unresolved field in the mesoscopic momentum transport equation of the dispersed phase, but also a stress term modeling the Random-Uncorrelated Motion is needed. Simulations of a non-homogeneous particle laden turbulent gas flow allow to compare dispersed phase quantities such as number density, time-averaged and rms mesoscopic velocity, fluid-particle correlations with experimental results.

Keywords: Large Eddy Simulation, Solid particle, Turbulent dispersion, Mesoscopic Velocity, Random Uncorrelated Motion

1 Introduction

Large Eddy Simulations (LES) are rapidly becoming a powerful tool to study flows in complex geometries. They have recently been applied with success to modern combustion devices ([4], [3], [1], [15], [20]), leading to new insights on the unsteady compressible gas flow and improved understanding of the physical phenomena involved. For a complete description of such systems, this promising method should be extended to two-phase flows, including fuel droplets. These two-phase flows are characterized by a high level of dynamic coupling and inertia effects that depend on the particle relaxation time. The present work is part of a project which develops an LES numerical tool for the simulation of two-phase reactive flows in industrial applications.
Commonly used Lagrangian tracking techniques are able to handle most of the complex physical processes. However, they are also known to be numerically expensive as they require a high particle number density to reach a minimum level of accuracy. Therefore, Lagrangian methods are not efficient for unsteady simulations of turbulent industrial flows in complex geometries.

A three dimensional unsteady Euler-Euler approach is proposed as an alternative to simulate two-phase flows. In this approach, the dispersed phase is treated similarly to the continuous gas phase. An averaging operator leads to a system of conservation equations very similar to the ones for the gas. Therefore, the gas phase algorithm may be used on the dispersed phase with the same numerical accuracy and computational efficiency.
Such an Euler-Euler approach has been validated for gas-particle homogeneous isotropic turbulence. Druzhini and Elghobashi (1999) [5] analysed the case of very low inertia particles following the carrier flow almost instantaneously. However their model reaches its limits when considering particles having response times larger than the Kolmogorov time scales. In this case and following Fevrier *et al.* (2005) [7], it is necessary to decompose the instantaneous particle velocity into two contributions. The Mesoscopic Eulerian Particle Velocity (MEPV) field represents the turbulent velocity field shared by all the particles at a given location, and is a transported variable. The Random Uncorrelated Velocity (RUV) represents a random velocity component that is not spatially correlated and identified with each particle of the system. An additional stress term which does not appear when using the volume filtering approach ([14]), must be included in the MEPV transport equation to account for this uncorrelated motion. However, this term can not be computed from the resolved variables and needs to be modeled. Fevrier *et al.* (2005) [7] proposed an a priori relation linking the mesoscopic kinetic energy to the total particle kinetic energy, showing that the Random Uncorrelated Motion (RUM) of the particles increases with inertia. It has been validated by Vance *et al.* (2004) [26] in a turbulent channel flow. Another modeling approach based on a transport equation for the Random Uncorrelated kinetic Energy (RUE) was developed by Kaufmann *et al.* (2004) [10] and validated on a temporally decreasing homogeneous isotropic turbulence. When performing Large Eddy Simulations that resolve only the energy contained in large scales, it is necessary to develop Subgrid Scales (SGS) models for the dipersed phase in analogy with the gaseous phase. Moreau *et al.* (2005) [12] recently proposed a Smagorinsky-like model.
The RUE models and SGS models should be validated by comparison with experiments on generic simple configurations, still containing all the physical processes involved by these models. When doing so, a particularly delicate aspect is the treatment of boundary conditions. Indeed, the determination of the inlet turbulent characteristics of the discrete phase is an open question.
The purpose of the present study is to evaluate the impact of different turbulent inlet boundary conditions in the gas-solid turbulent confined jet experimentally investigated by Hishida *et al.* (1987) [9]. In this configuration, light hollow glass particles with a Stokes number (based on the most energetic eddies of the turbulence) of 0.4 are transported by a jet with a Reynolds number of 22000 in gravitationnal direction without a recirculating flow. Two-phase flow simulations have been performed with three different formulations of the turbulent inlet boundary conditions for the discrete phase. In the first case, no particle turbulent mesoscopic kinetic energy is injected. For the two other cases, the basic idea is that the turbulent inlet particle velocity field is partially correlated to the gas one. Therefore, two boundary conditions are written for the dispersed phase that verify both a given turbulent kinetic energy and a given fluid-particle correlation at the inlet. Only the two first cases are reported in this work. Results clearly show that the particle mass flux highly depends on the inlet dispersed phase boundary condition. However, neither the radial nor the axial turbulent mesoscopic energy seems to be much affected, only in the near-inlet region. Using the correlation validated by Vance *et al.* (2004) [26] confirms

that the part of kinetic energy residing in the RUM is more than non-negligible in this configuration.

2 The Euler-Euler model

2.1 The dispersed phase

Eulerian equations for the dispersed phase may be derived by several means. A popular and simple way consists of volume filtering of the separate, local, instantaneous phase equations accounting for the inter-facial jump conditions ([6], [14]). Such an averaging approach is very restrictive, because particle sizes and particle distances have to be smaller than the smallest length scale of the turbulence. Besides, they do not account for the Random Uncorrelated Motion ([7]).
A different, not totally equivalent way is the statistical approach in the framework of kinetic theory. In analogy to the derivation of the Navier-Stokes equations by kinetic theory [2], a probability density function (pdf) $f_p^{(1)}(\mathbf{c}_p; \mathbf{x}_p, t)$ may be defined. This gives the local instantaneous probable number of particles with the given translation velocity $\mathbf{u}_p = \mathbf{c}_p$. This function obeys a Boltzmann-type kinetic equation that accounts for momentum exchange with the carrier fluid and for the influence of external forces such as gravity and inter-particle collisions. Transport equations of the first moments (such as particle concentration, mean velocity and particle kinetic stress) may be derived directly by averaging from the pdf kinetic equation [21].
For the sake of simplicity, in this study interaction forces are limited to drag and gravity, and only non-evaporating particles are considered. The extension to evaporating flows, turbulence corrections in the drag force and other interaction forces is not in conflict with the presented derivation of the Eulerian field equations. In the presented approach, the gas is presumed undisturbed by the dispersed phase.

2.1.1 Mesoscopic Conservation Equations for particle properties

To derive local instantaneous Eulerian equations in dilute flows (without turbulence modification by the particles), Février *et al.* (2005) [7] propose to use an averaging over all dispersed-phase realizations conditioned by one carrier-phase realization. Such an averaging procedure leads to a conditional velocity pdf for the dispersed phase, $\breve{f}_p^{(1)}(\mathbf{c}_p; \mathbf{x}, t, H_f)$, defining the local probable number of particle centers at the position $\boldsymbol{x}$, with a given translation velocity $\boldsymbol{v}_p = \boldsymbol{c}_p$ at time t :

$$\breve{f}_p^{(1)}(\mathbf{c}_p; \mathbf{x}, t, H_f) = \left\langle W_p^{(1)}(\mathbf{c}_p; \mathbf{x}, t) \,|H_f \right\rangle \tag{1}$$

$W_p^{(1)}$ are the realizations of position and velocity in time of any given particle ([18]) and H_f is the unique carrier flow realization. With this definition one may define a local instantaneous particulate velocity field, which is here named "Mesoscopic Eulerian Particle Velocity (MEPV) field". This field is obtained by averaging the conditioned velocity pdf over all particle-flow realizations :

$$\breve{\mathbf{u}}_p(\mathbf{x}, t, H_f) = \frac{1}{\breve{n}_p(\mathbf{x}, t, H_f)} \int \mathbf{c}_p \breve{f}_p^{(1)}(\mathbf{c}_p; \mathbf{x}, t, H_f)\, d\mathbf{c}_p \tag{2}$$

Eq. (3) gives the "mesoscopic" particle-number density and Eq. (4) defines any ensemble averaged quantity :

$$\breve{n}_p(\mathbf{x},t,H_f) = \int \breve{f}_p^{(1)}(\mathbf{c}_p;\mathbf{x},t,H_f)\,d\mathbf{c}_p \tag{3}$$

$$\langle\breve{\Phi}\rangle(\mathbf{x},t,H_f) = \frac{1}{\breve{n}_p(\mathbf{x},t,H_f)}\int \breve{f}_p^{(1)}(\mathbf{x},t,H_f)\,\Phi d\mathbf{c}_p \tag{4}$$

Application of the conditional-averaging procedure to the kinetic equation governing the particle pdf leads directly to the transport equations for the first moments of number density and Mesoscopic Eulerian Partcile Velocity,

$$\frac{\partial}{\partial t}\breve{n}_p + \frac{\partial}{\partial x_i}\breve{n}_p\breve{u}_{p,i} = 0 \tag{5}$$

$$\frac{\partial}{\partial t}\breve{n}_p\breve{u}_{p,i} + \frac{\partial}{\partial x_j}\breve{n}_p\breve{u}_{p,j}\breve{u}_{p,i} = \frac{\partial}{\partial x_j}\breve{\tau}_{p,ij} - \frac{\partial}{\partial x_i}\left(\frac{2}{3}\breve{n}_p\delta\breve{\theta}_p\right) - \frac{\breve{n}_p}{\tau_p}(\breve{u}_{p,i}-u_{f,i}) + \breve{n}_p g_i. \tag{6}$$

Due to the very small droplet Reynolds number value measured in the simulation, the particle relaxation time τ_p is defined as the relaxation time for Stokes drag :

$$\tau_p = \frac{\rho_p d^2}{18\mu} \tag{7}$$

In Eq. (6), the Random Uncorrelated stress tensor, $\breve{\tau}_{p,ij}$ reads :

$$\breve{\tau}_{p,ij} = -\breve{n}_p\langle\delta u_{p,i}\delta u_{p,j}\rangle_p + \frac{2}{3}\breve{n}_p\delta\breve{\theta}_p\delta_{i,j} \tag{8}$$

where $\langle\delta u_{p,i}\delta u_{p,j}\rangle_p$ is the mesoscopic kinetic stress tensor of the particle velocity distribution and $\delta\breve{\theta}_p$ is the RUM kinetic energy defined as:

$$\delta\breve{\theta}_p = \frac{1}{2}\langle\delta u_{p,i}\delta u_{p,i}\rangle_p \tag{9}$$

Modelisation of $\breve{\tau}_{p,ij}$ is part of Section 2.3.1.

Using the mean particle velocity $\mathbf{U}_p(\mathbf{x},t)$, the mesoscopic fluctuating particle velocity is defined by :

$$\mathbf{u}'_p(t) = \breve{\mathbf{u}}_p(t) - \mathbf{U}_p(\mathbf{x},t) \tag{10}$$

Using Eq. (10), the particle mesoscopic integral kinetic energy, $\breve{q}_p^2$ and the fluid-particle correlation, q_{fp} are then expressed by :

$$\breve{q}_p^2 = \frac{1}{2}\langle u'_{p,i}(t)u'_{p,i}(t)\rangle \tag{11}$$

$$\breve{q}_{fp} = \langle u'_{p,i}(t)u'_{f,i}(t)\rangle \tag{12}$$

where $u'_{f,i}$ is the fluid velocity fluctuation at the particle location. The fluid integral kinetic energy, q_f^2 reads :

$$q_f^2 = \frac{1}{2}\langle u'_{f,i}(t)u'_{f,i}(t)\rangle \tag{13}$$

2.1.2 Filtered Conservation Equations for particle properties

In LES, the filtering procedure consists in defining averaged variables that are obtained by a convolution product of the unfiltered variable f with a filter kernel F. Typical examples for filtering kernels are top hat filters or Gaussian functions with the corresponding filtering kernel in spectral space ([19], [8], [16]). A filtered quantity $\bar{f}$ is defined as :

$$\bar{f}(x) = \int f(x) F(x' - x) dx' \tag{14}$$

When studying flows with varying density, it is common practice to define Favre averaged quantities. The Favre filtered quantity reads :

$$\bar{\rho}\tilde{f}(x) = \int \rho(x) f(x) F(x' - x) dx' \tag{15}$$

Dealing with particles leads to replace the gas density ρ with the density number n_p.

This filtering procedure is applied to the conservation equations of the dispersed phase obtained from the ensemble averaging procedure (see Section 2.1.1). The conservation equations for the filtered dispersed phase are :

$$\frac{\partial}{\partial t}\bar{n}_p + \frac{\partial}{\partial x_j}\bar{n}_p\tilde{u}_{p,j} = 0 \tag{16}$$

$$\begin{aligned}\frac{\partial}{\partial t}\bar{n}_p\tilde{u}_{p,i} + \frac{\partial}{\partial x_j}\bar{n}_p\tilde{u}_{p,i}\tilde{u}_{p,j} &= \frac{\partial}{\partial x_j}\tilde{\tau}_{p,ij} - \frac{\partial}{\partial x_i}\left(\frac{2}{3}\bar{n}_p\delta\tilde{\theta}_p\right) \\ &\quad - \frac{\bar{n}_p}{\tau_p}(\tilde{u}_{p,i} - \tilde{u}_{f,i}) + \bar{n}_p g_i - \frac{\partial}{\partial x_j}T_{p,ij,SGS}\end{aligned} \tag{17}$$

For the sake of simplicity, the mesoscopic sign has been omitted in Eqs. (16) & (17). The filtered dispersed phase equations contain one unclosed term, $T_{p,ij,SGS}$ that is due to filtering. Its modelisation is discussed in Section 2.3.2.

2.2 The gas phase

Here, the filtering procedure described in Section 2.1.2 is applied to the compressible Navier-Stokes equations. The filtered conservation equations for the gas phase are :

$$\frac{\partial}{\partial t}\bar{\rho} + \frac{\partial}{\partial x_j}\bar{\rho}\tilde{u}_{f,j} = 0 \tag{18}$$

$$\frac{\partial}{\partial t}\bar{\rho}\tilde{u}_{f,i} + \frac{\partial}{\partial x_j}\bar{\rho}\tilde{u}_{f,i}\tilde{u}_{f,j} = -\frac{\partial}{\partial x_i}\bar{P} + \frac{\partial}{\partial x_j}\bar{\tau}_{ij} - \frac{\partial}{\partial x_j}T_{ij,SGS} \tag{19}$$

$$\frac{\partial}{\partial t}\bar{\rho}\tilde{E} + \frac{\partial}{\partial x_j}\bar{\rho}\tilde{E}\tilde{u}_{f,j} = \frac{\partial}{\partial x_j}\overline{(-P + \tau_{ij})u_{f,i}} + \frac{\partial}{\partial x_j}q_{SGS} \tag{20}$$

where $\bar{\rho}$ is the Favre filtered density, $\tilde{u}_i$ is the resolved velocity field, P is the pressure, τ_{ij} is the viscous tensor, E is the total non-chemical energy, $T_{ij,SGS}$ is the Reynolds tensor and q_{SGS} is the Sub-Grid Scale heat flux vector. The treatment of these two unclosed terms is discussed in Section 2.3.2.

2.3 Modeling the unclosed terms

2.3.1 The unresolved Random Uncorrelated kinetic Stresses $\langle \delta u_{p,i} \delta u_{p,j} \rangle_p$

When computing a temporally decreasing homogeneous isotropic turbulence, Fevrier *et al.* (2005) [7] showed that the ratio of Random Uncorrelated kinetic Energy (RUE) to total particle kinetic energy increases with particle inertia. They proposed a relation which Vance *et al.* (2004) [26] extended to a turbulent channel flow that reads :

$$< \delta u_{p,i} \delta u_{p,i} >_p = < \tilde{u}'_{p,i} \tilde{u}'_{p,i} >_p \left(\frac{< \tilde{u}'_{p,i} \tilde{u}'_{p,i} >_p < \tilde{u}'_{f,i} \tilde{u}'_{f,i} >_f}{< \tilde{u}'_{f,i} \tilde{u}'_{p,i} >_p^2} - 1 \right) \tag{21}$$

Another modeling approach based on a transport equation for the Random Uncorrelated kinetic Energy was proposed by Simonin *et al.* (2002) [22] and validated by Kaufmann *et al.* (2004) [10] on a temporally decreasing homogeneous isotropic turbulence.

This term is however not taken into account in the equations resolved in this paper. Its influence will be part of future work. In this work, Eq. (21) is only used *a posteriori* to compute the RUE .

2.3.2 The unresolved Sub-Grid terms $T_{k,ij,SGS}$ and q_{SGS}

For each phase noted k, the filtered equations exhibit Sub-Grid Scales (SGS) tensors and vectors that describe the interaction between the non-resolved and resolved motions. The influence of the SGS on the resolved motion is taken into account by a SGS model based on the introduction of a turbulent viscosity,$\nu_{k,SGS}$.
For both phases, the LES-filtered Boussinesq tensor $\tilde{S}_{k,ij}$ and the LES-filtered Boussinesq tensor without trace $\tilde{S}^*_{k,ij}$ are defined as :

$$\tilde{S}_{k,ij} = \frac{1}{2} \left(\frac{\partial}{\partial x_j} \tilde{u}_{k,i} + \frac{\partial}{\partial x_i} \tilde{u}_{k,j} \right) \tag{22}$$

$$\tilde{S}^*_{k,ij} = \tilde{S}_{k,ij} - \frac{1}{3} \tilde{S}_{k,mm} \delta_{ij} \tag{23}$$

• The gas phase

Ducros & Nicoud (1999) [13] developped a Wall-Adaptating Local Eddy-viscosity (WALE) model for $T_{ij,SGS}$ based on the Smagorinsky model [23]. The difference is in the definition of the turbulent viscosity, ν_{SGS} that differs from the Smagorinsky model, leading to less dissipative flows and more accurate behaviour at the wall. The Reynolds Tensor $T_{ij,SGS}$ is defined as:

$$T_{ij,SGS} = \bar{\rho}(\widetilde{u_i u_j} - \tilde{u}_i \tilde{u}_j) \tag{24}$$

$$T_{ij,SGS} = -\nu_{SGS} \tilde{S}^*_{ij} \tag{25}$$

where ν_{SGS} reads :

$$\nu_{SGS} = (C_w \Delta_f)^2 \frac{\left(s^d_{f,ij} s^d_{f,ij} \right)^{\frac{3}{2}}}{\left(\tilde{S}_{f,ij} \tilde{S}_{f,ij} \right)^{\frac{5}{2}} + \left(s^d_{f,ij} s^d_{f,ij} \right)^{\frac{5}{4}}} \tag{26}$$

with $s^d_{f,ij} = \frac{1}{2}\left(\left[\frac{\partial}{\partial x_i}\tilde{u}_{f,j}\right]^2 + \left[\frac{\partial}{\partial x_j}\tilde{u}_{f,i}\right]^2\right) - \frac{1}{3}\left[\frac{\partial}{\partial x_k}\tilde{u}_{f,k}\right]^2 \delta_{ij}$. $C_w = 0.4929503$ is the model constant and Δ_f denotes the filter characteristic length.
Then the Sub-Grid Scale heat flux vector q_{SGS} follows :

$$q_{SGS} = \frac{\gamma}{P_r^{SGS}} \bar{\rho}\nu_{SGS} \nabla\left(\tilde{E} - \tilde{u_i^2}\right) \tag{27}$$

where γ is the gas constant and $P_r^{SGS} = 0.9$ is the subgrid Prandtl number.

• The dispersed phase

Moreau *et al.* (2005) [12] developed a SGS model in analogy to the one developped by Moin & al. (1991) [11] for compressible flows :

$$T_{p,ij,SGS} = \breve{\bar{n}}_p(\breve{u}_{p,i}\widetilde{\breve{u}_{p,j}} - \tilde{\breve{u}}_{p,i}\tilde{\breve{u}}_{p,j}) \tag{28}$$

$$T_{p,ij,SGS} = P_{p,SGS}\delta_{ij} - \nu_{p,SGS}\tilde{\breve{S}}^*_{p,ij} \tag{29}$$

Following respectively Yoshizawa (1986) [27] and Smagorinsky (1963) [23], $P_{p,SGS}$ and $\nu_{p,SGS}$ are defined as:

$$P_{p,SGS} = 4\, C_l\, \breve{\bar{n}}_p\, \Delta_f^2\, \tilde{\breve{S}}_{p,ij}\tilde{\breve{S}}_{p,ij} \quad with\ \ C_l = 0.012 \tag{30}$$

$$\nu_{p,SGS} = 4\, C_S\, \breve{\bar{n}}_p\, \Delta_f^2 \sqrt{\tilde{\breve{S}}_{p,ij}\tilde{\breve{S}}_{p,ij}} \quad with\ \ C_S = 0.02 \tag{31}$$

3 Description of the configuration and the numerical test cases

3.1 Description of the configuration

The effect of solid particles on the flow structure of a confined jet was experimentally investigated by Hishida *et al.* (1987) [9]. Figure 1 illustrates the configuration. The jet from a tube of diameter $D_2 = 0.13mm$ (named T_2) is confined with a tube of diameter $D_1 = 0.6mm$ (named T_1). Spherical light hollow glass particles of diameter $d = 80.1\mu m$ are loaded with a constant volume fraction. The Reynolds number is 22000 at the outlet of the confined jet and the flow direction is parallel to the gravity vector. A laser Doppler velocimeter system was used to measure both two-component velocities of gas and particles, and their fluctuations at three different positions in the tube : z=0m, z=$10D_2$ and z=$20D_2$.

3.2 Numerical aspects

The LES solver AVBP_TPF (see www.cerfacs.fr/cfd/CFDWeb.html) solves the full compressible Navier Stokes equations for the gas phase and the full mesoscopic conservation equations for the dispersed phase on hybrid (structures and unstructured) grids. The numerical scheme uses third-order spatial accuracy and third-order temporal accuracy [3]. As acoustics is part of the gas equations, characteristic boundary conditions are used for the

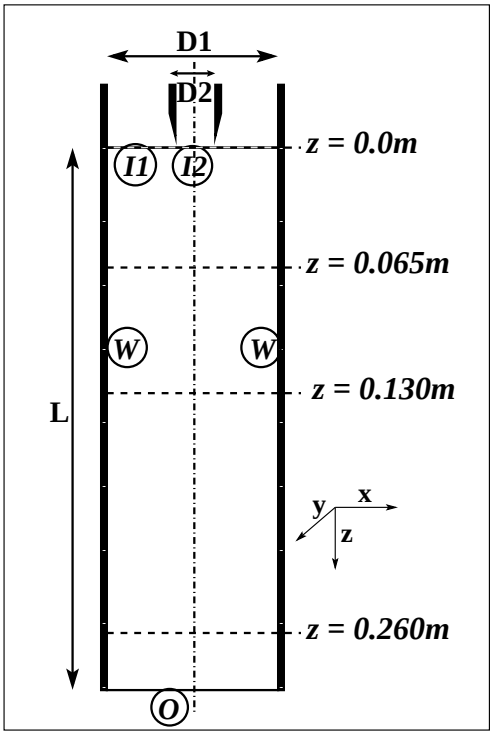

Figure 1: Sketch

gas phase (see [17]). Dirichlet-like boundary conditions are used for the dispersed phase. Zero gas velocity is imposed on the walls of the tube T_2 whereas they are considered as slipping walls for the particles. The static pressure is imposed at the outlet. At the main duct inlet (Patch I2 in Fig. 1), the values of $\tilde{u_{f,i}}$, i$\in$[1,3] vary in time and space to reproduce the effect of an incoming turbulent field as observed in the experiment. The method in constructing the incoming turbulent signal is based on the Random Flow Generation (RFG) algorithm [24], [25]. The continuously homogeneous isotropic incoming field consists of a superposition of harmonic functions (50 modes projected in the three directions) with characteristic length-scales prescribed by the user. Forcing the flow in such a way considerably accelerates the establishment of fully developed turbulent flows. It also ensures the presence of coherent perturbations not warranted when a pure white noise is used. Special treatments for particles on the same patch $I2$ are discussed in Section 3.3. Typical runs are performed on grids of 520,000 structured elements on 48 processors.

3.3 The numerical test cases

The experiments show that the particle velocity field is turbulent at the outlet of the tube T_2. This work aims at determining the influence of the inlet boundary condition on the flow. At the inlet, the turbulent particle mesoscopic velocity field is known to be partially correlated to the gas turbulent velocity field. A simple way to account for this correlation is to suppose that the turbulent mesoscopic particle velocity field is divided into two contributions (see Eq. (32)).

$$\tilde{u}'_{p,i} = A\tilde{u}'_{f,i} + B\tilde{w}'_i \tag{32}$$

Both fields, $\tilde{u}'_{f,i}$ and $\tilde{w}'_i$, are generated the same way (same characteristic length scales). The first one, $\tilde{u}'_{f,i}$, is directly collinear to the turbulent gas velocity field. The second contribution, $\tilde{w}'_i$, is completely decorrelated from the gas field and has no physical sense. Then, the coefficients A and B from Eq. (32) are determined so as to ensure both a given total particle turbulent kinetic energy and a given fluid-particle correlation :

$$(\tilde{u}'_{p,i})^2 = A^2(\tilde{u}'_{f,i})^2 + B^2(\tilde{w}'_i)^2 \quad (33)$$

$$\tilde{u}'_{p,i}\tilde{u}'_{f,i} = A(\tilde{u}'_{f,i})^2 \quad (34)$$

Such an approach allows to define several inlet boundary conditions for the particles. Three of them are tested in this work :

	$\tilde{q}_p^2$	$\tilde{q}_{fp}$	A	B
BC1	0	0	0	0
BC2	q_p^2	$2A\tilde{q}_f^2$	$\sqrt{\frac{q_p^2}{q_f^2}}$	0
BC3	q_p^2	0	0	$\sqrt{\frac{q_p^2}{q_f^2}}$

Table 1: Description of the different boundary conditions tested for the disperse phase.

where q_p^2 is the particle turbulent kinetic energy experimentally measured.

The influence of the two first inlet boundary conditions on the particle flow is presented and discussed in Section 4. For both cases, the Random Uncorrelated kinetic Energy is computed *a posteriori* (see Eq. (21)).

4 Results and Discussion

Comparisons between the experiments and the simulations are made in three different plans perpendicular to the duct axis and located at the positions : z=0, z=$10D_2$ and z=$20D_2$ where D_2 is the diameter of tube T_2. A fourth plan with position z=$5D_2$ is added to obtain more information. LES data are averaged over about 26 ms corresponding to two flow times through the entire domain at the bulk velocity. For both phases, the mean axial $< W_k >$ and radial velocities $< Vr_k >$ are plotted as well as the rms axial $< w_{k,rms} >$ and radial $< vr_{k,rms} >$ velocities and the turbulent kinetic energy. The particle mass flux is also considered. To do so, the field is spatially averaged in the circumferential direction. As the influence of the particles on the gas flow is not taken into account, results for the gas phase are presented in Section 4.1. Sections 4.2.1 and 4.2.2 focus on the dispersed phase for the two first boundary conditions summarized in Table 1.

4.1 Gas phase

Figure 2 compares PDPA measurements (symbols) with averaged LES results (lines) at the four downstream locations z in the tube for the gas phase. The overall agreement between LES and experimental data is very good. The spreading of the turbulent jet is

well predited, as well as the mean and fluctuating velocity levels. Concerning the RMS profiles (Fig. 2 c. & d.), only the resolved part of the fluctuations is taken into account here. This shows that for this flow, most of the unsteady motion lies in large structures which are well predicted by LES methods.

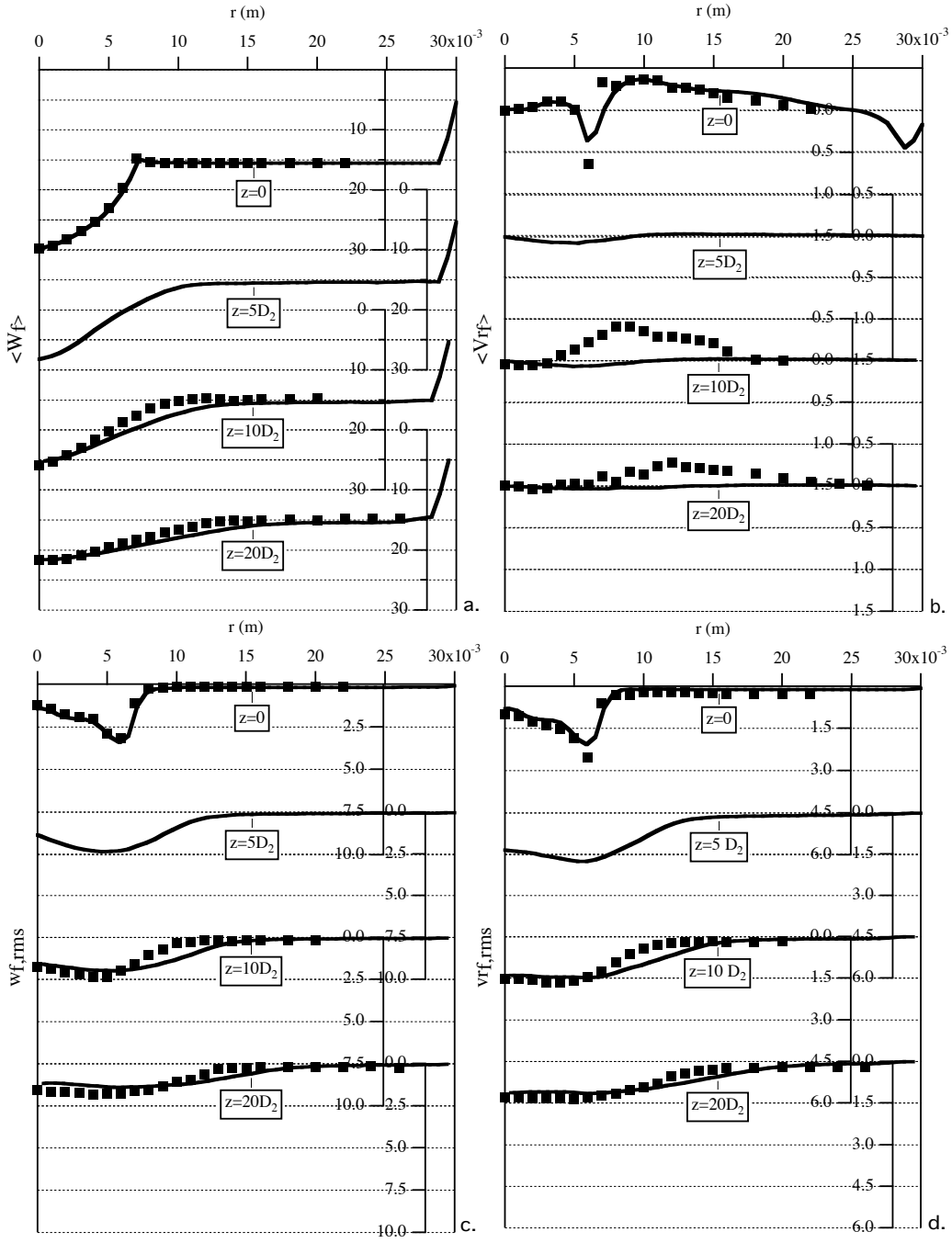

Figure 2: Gas phase ; comparison between time-averaged LES results (lines) and experimental results (symbols) of a. and b., mean axial and radial velocity profiles, c. and d., turbulent axial and radial velocity profiles.

4.2 Dispersed phase

4.2.1 BC1

This Section presents the results obtained for the dispersed phase when using the first boundary condition described in Table 1. In this case, no turbulent mesoscopic kinetic energy is injected at the inlet of the domain.

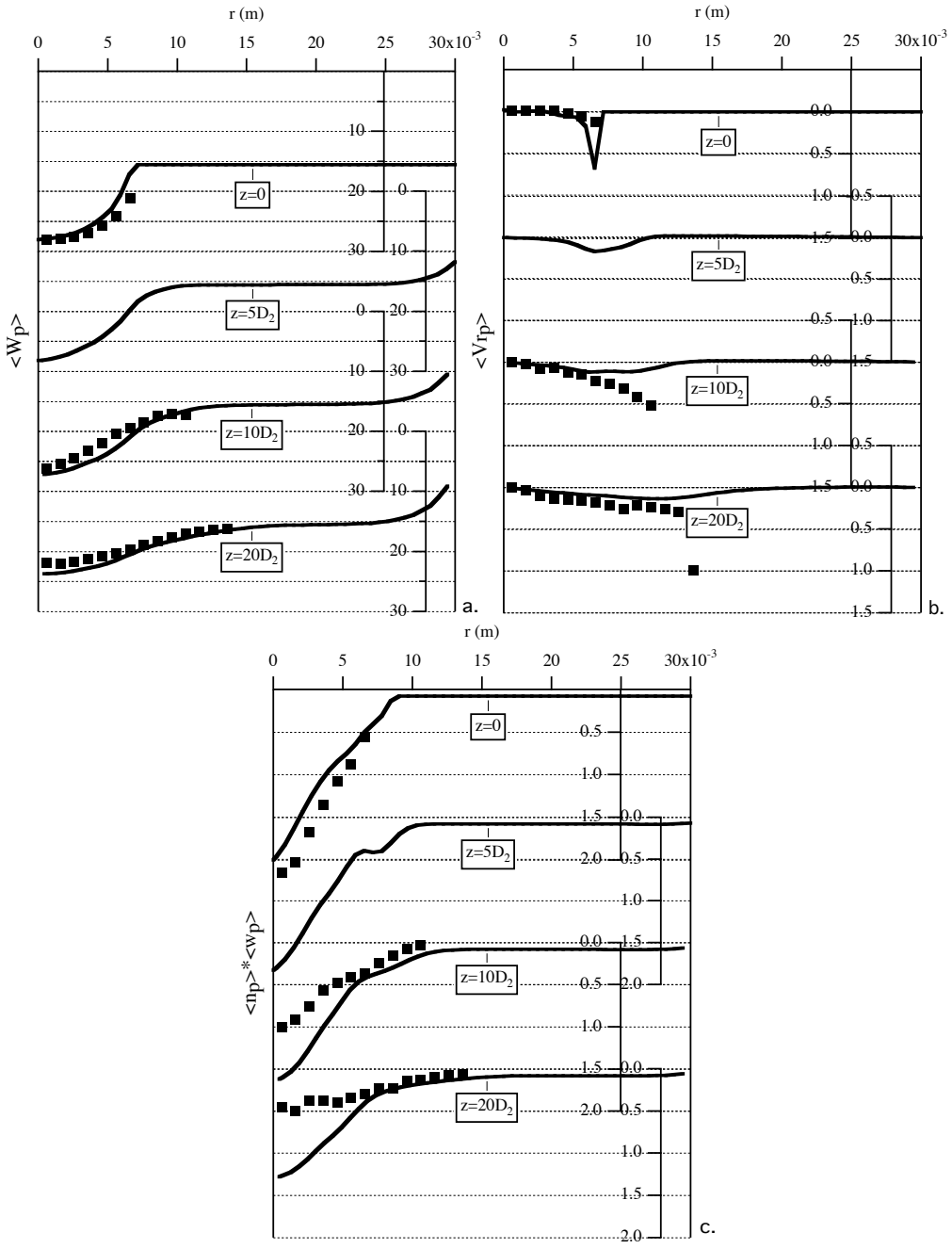

Figure 3: Dispersed phase - BC1 ; comparison between time-averaged LES results (lines) and experimental results (symbols) of a., mean axial velocity profiles, b., mean radial velocity profiles, and c., mean mass flux profiles.

Figure 3 compares PDPA measurements (symbols) with averaged LES results (lines) at the four downstream locations z in the tube for mean quantities. The mean axial and radial velocity levels are well predicted. Considering the mass flux profile, the particles are not dispersed enough. Figure 4 compares the square rms axial and radial velocities (lines) with both the fluid-particle correlations (dashed lines) and the Random Uncorrelated kinetic Energy (dot-dashed lines). Experimentally, the radial fluctuations are much smaller than the axial fluctuations. This is also the case for the LES predictions although both fluctuations are considerably under-estimated. The fluid-particle correlation levels show that the numerical scheme used is still a little too much dissipative. Whatever the position in the tube, the radial fluid-particle correlation is greater than the square rms radial fluctuations. Finally, the Random Uncorrelated Motion is consequent in both directions.

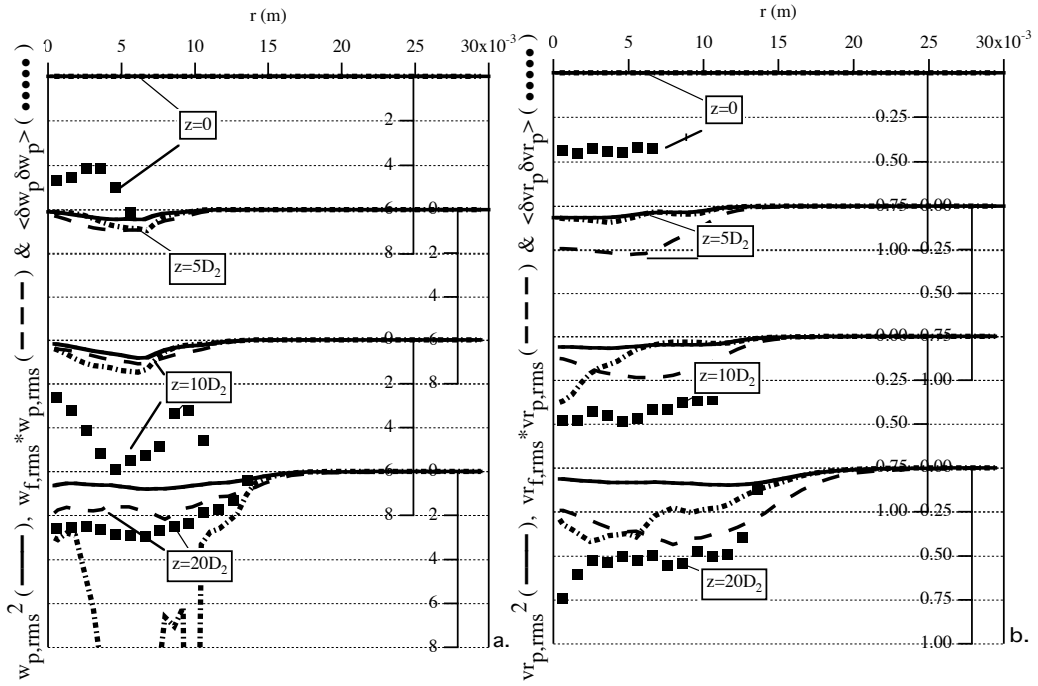

Figure 4: Dispersed phase - BC1 ; Time-averaged LES results for the square rms velocities (lines), the fluid-particle correlation (dashed lines) and the *a posteriori* computed Random Uncorrelated kinetic Energy (dot-dashed lines) compared to the experimental velocity fluctuations ; a., axial profiles and b., radial profiles.

4.2.2 BC2

Figures 5 and 6 compare PDPA measurements (symbols) with averaged LES results (lines) for the dispersed phase when BC2 is used at the inlet. In this case, the particle fluctuations are colinear to the gas ones, which explains that the particle fluctuations imposed at the inlet are isotropic. Therefore, the computed total particle kinetic energy corresponds to the experimental one at the inlet but the distribution in space does not match the experiments since the particle fluctuations are very anisotropic. The mesoscopic fluctuations at the inlet do not affect much axial and radial mean and fluctuating velocities along the tube, only in the near-inlet region. However, the mass flux is much more sensitive to the boundary

condition and the particles are much more dispersed in this case. Considering Figure 6, the Random Uncorrelated kinetic Energy (dot-dashed lines) is more than non-negligible compared to the rms velocities. This partly explains the lack of rms axial and radial velocities in comparison with the experimental results. Once more, the radial fluid-particle correlation is greater than the square rms radial fluctuations.

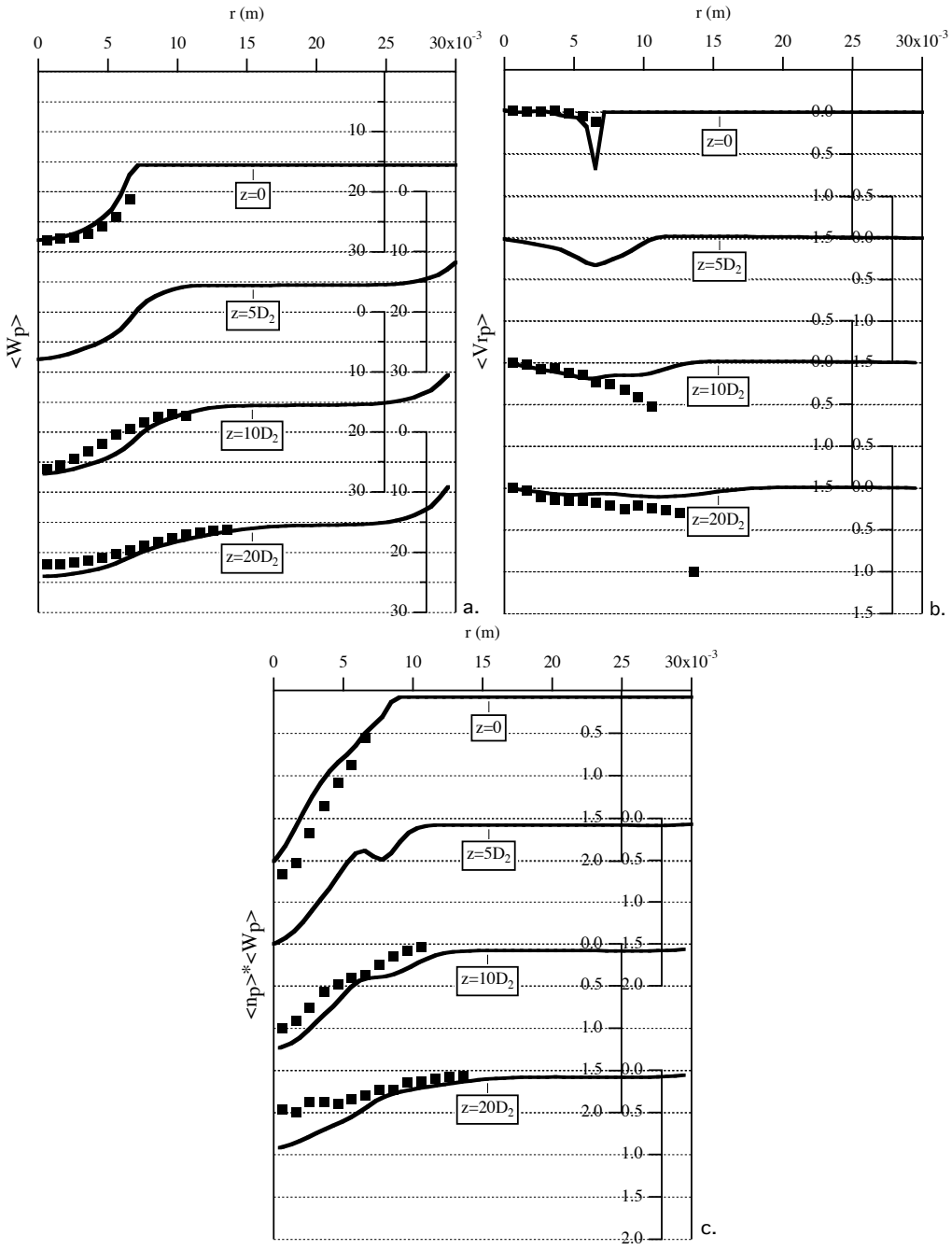

Figure 5: Dispersed phase - BC2 ; comparison between time-averaged LES results (lines) and experimental results (symbols) of a., mean axial velocity profiles, b., mean radial velocity profiles, and c., mean mass flux profiles.

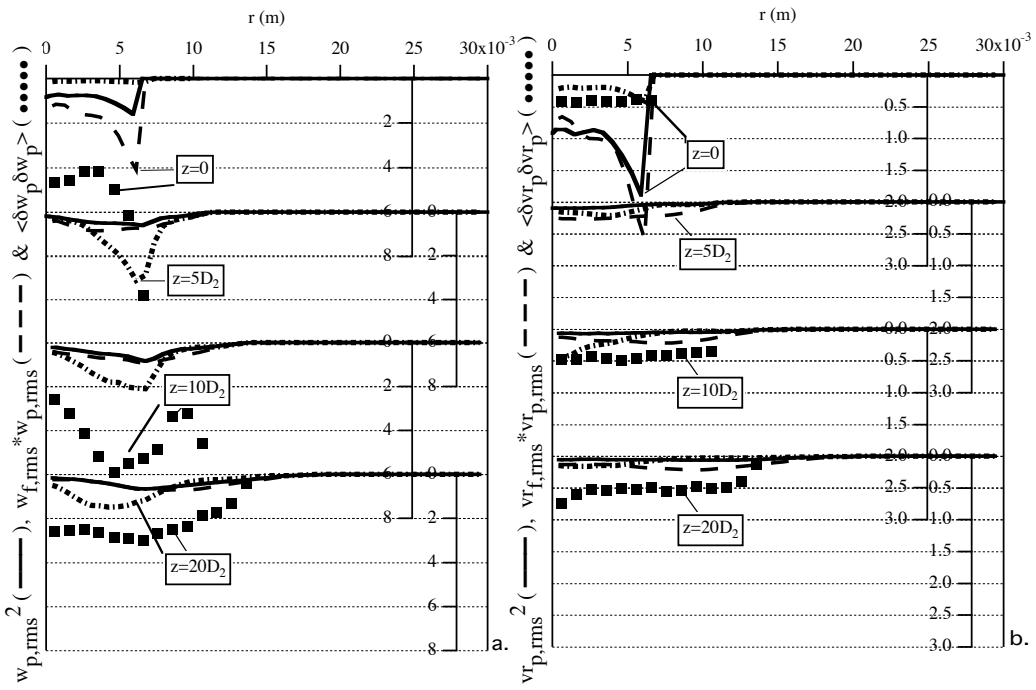

Figure 6: Dispersed phase - BC2 ; Time-averaged LES results for the square rms velocities (lines), the fluid-particle correlation (dashed lines) and the *a posteriori* computed Random Uncorrelated kinetic Energy (dot-dashed lines) compared to the experimental velocity fluctuations ; a., axial profiles and b., radial profiles.

5 Conclusion and prospectives

The presented study shows the capacity of Euler-Euler model to simulate the dynamics of particles in a confined jet. The treatment of the inlet boundary condition seems to have a great influence on the particle mass flux. It seems important to also model the Random Uncorrelated Motion to predict correctly the particle fluctuating motion.

References

[1] C. Angelberger C, F. Egolfopoulos, and D. Veynante. Large eddy simulations of chemical and acoustic effects on combustion instabilities. *Flow, Turbulence and Combustion*, 65(2):205–222, 2000.

[2] S. Chapman and T.G. Cowling. *The Mathematical Theory of Non-Uniform Gases*. Cambridge University Press, cambridge mathematical library edition, 1939 (digital reprint 1999).

[3] O. Colin, F. Ducros, D. Veynante, and T. Poinsot. A thickened flame model for large eddy simulations of turbulent premixed combustion. *Physics of Fluids*, 12(7):1843–1863, 2000.

[4] P. E. Desjardins and S. H. Frankel. Two dimensional large eddy simulation of soot formation in the near field of a strongly radiating nonpremixed acetylene-air jet flame. *Combustion and Flame*, 119/(1/2):121–133, 1999.

[5] O.A. Druzhini and S. Elghobashi. Direct numerical simulations of bubble-laden turbulent flows using the two-fluid formulation. *Physics of Fluids*, 10(3):685–697, 1998.

[6] O.A. Druzhini and S. Elghobashi. On the decay rate of isotropic turbulence laden with microparticles. *Physics of Fluids*, 11(3):602–610, 1999.

[7] P. Février, O. Simonin, and K. Squires. Partitioning of particle velocities in gas-solid flows into a continuous field and a spatially-uncorrelated random distribution: theoretical formalism and numerical study. *Journal of Fluid Mechanics, in press*, 2005.

[8] M. Germano. Turbulence: the filtering approach. *Journal of Fluid Mechanics*, 238:325–336, 1992.

[9] K. Hishida, K. Takemoto, and M. Maeda. Turbulent characteristics of gas-solids two-phase confined jet. *Japanese Journal of Multiphase Flow*, 1(1):56–69, 1987.

[10] A.. Kaufmann, O. Simonin, and T. Poinsot. Direct numerical simulation of particle-laden homogeneous isotropic turbulent flows using a two-fluid model formulation. In *5^{th} Int. Conf. on Multiphase Flow*. ICMF'04, 2004.

[11] P. Moin, K. Squires, W. Cabot, and S. Lee. A dynamic subgrid-scale model for compressible turbulence and scalar transport. *Physics of Fluids*, A 3(11):2746–2757, 1991.

[12] M. Moreau, B. Bedat, and O. Simonin. From euler-lagrange to euler-euler large eddy simulation approaches for gas-particle turbulent flows. In *ASME Fluids Engineering Summer Conference*. ASME FED, 2005.

[13] F. Nicoud and F. Ducros. Subgrid-scale stress modelling based on the square of the velocity gradient tensor. *Flow, Turbulence and Combustion*, 62(3):183–200, 1999.

[14] R.V.R. Pandya and F. Mashayek. Two-fluid large-eddy simulation approach for particle-laden turbulent flows. *International Journal of Heat and Mass Transfer*, 45:4753–4759, 2002.

[15] C. D. Pierce and P. Moin. Progress-variable approach for large eddy simulation of non-premixed turbulent combustion. *Journal of Fluid Mechanics*, 504:73–97, 2004.

[16] U. Piomelli. Large-eddy simulation: achievements and challenges. *Progress in Aeorspace Sciences*, 35:335–362, 1999.

[17] T. Poinsot and S. Lele. Boundary conditions for direct simulations of compressible viscous flows. *Journal of Computational Physics*, 101(1):104–129, 1992.

[18] M.W. Reeks. On a kinetic equation fo the transport of particles in turbulent flows. *Physics of Fluids A*, 3(3):446–456, 1991.

[19] Pierre Sagaut. *Introduction à la simulation des grandes échelles*. Springer, mathématiques & applications edition, 1998.

[20] L. Selle, G. Lartigue, T. Poinsot, R. Koch, K-U. Schildmacher, W. Krebs Wand B. Prade B, P. Kaufmann, and D. Veynante. Compressible large-eddy simulation of turbulent combustion in complex geometry on unstructured meshes. *Combustion and Flame*, 137/(4):489–505, 2004.

[21] O. Simonin. Combustion and turbulence in two phase flows. Lecture Series 1996-02, von Karman Institute for Fluid Dynamics, 1996.

[22] O. Simonin, P. Fevriér, and J. Laviéville. On the spatial distribution of heavy particle velocities in turbulent flow: from continous field to particulate choas. *Journal of Turbulence*, 3:040, 2002.

[23] J. Smagorinsky. General circulation experiments with the primitive equations. i: The basic experiment. *Monthly Weather Review*, 91(3):99–165, 1963.

[24] A. Smirnov, S. Shi, and I. Celik. Random flow generation technique for large eddy simulations and particle-dynamics modeling. *Journal of Computational Physics*, 2000.

[25] E. Van Kalmthout, T. Poinsot, and S. Candel. Turbulence, théorie et simulations directes. Technical Report TR/CFD/95/39, Laboratoire E.M2.C Ecole Centrale de Paris, 1995.

[26] M.W. Vance, K.D. Squires, and O. Simonin. Properties of the particle velocity field in gas-solid turbulent channel flow. In 5^{th} *Int. Conf. on Multiphase Flow*. ICMF'04, 2004.

[27] A. Yoshizawa. Statistical theory for compressible turbulent shear flows, with the application to subgrig modeling. *Physics of Fluids*, 29(7):2152–2164, 1986.